



Contents lists available at SciVerse ScienceDirect

Journal of Controlled Release

journal homepage: www.elsevier.com/locate/jconrel

Thermally-triggered ‘off-on-off’ response of gadolinium-hydrogel–lipid hybrid nanoparticles defines a customizable temperature window for non-invasive magnetic resonance imaging thermometry

Adam J. Shuhendler^a, Robert Staruch^{b,c}, Wendy Oakden^{b,c}, Claudia R. Gordijo^a, Andrew M. Rauth^{b,d}, Greg J. Stanisz^{b,c}, Rajiv Chopra^{b,c}, Xiao Yu Wu^{a,*}

^a Department of Pharmaceutical Sciences, Leslie L. Dan Faculty of Pharmacy, University of Toronto, Toronto, Ontario, Canada M5S 3M2

^b Department of Medical Biophysics, University of Toronto, Toronto, Ontario, Canada M5G 2M9

^c Imaging Research, Sunnybrook Research Institute, Sunnybrook Health Sciences Centre, Toronto, Ontario, Canada M4N 3M5

^d Ontario Cancer Institute, Princess Margaret Hospital, University Health Network, Toronto, Ontario, Canada M5G 2C5

ARTICLE INFO

Article history:

Received 11 June 2011

Accepted 6 September 2011

Available online 10 September 2011

Keywords:

Magnetic resonance imaging
Thermometry
Hydrogel–lipid hybrid nanoparticles
T1-weighted
Temperature responsive contrast agent
Thermotherapy

ABSTRACT

For effective and safe thermotherapy, real-time, accurate, three-dimensional tissue thermometry is required. Magnetic resonance imaging (MRI)-based thermometry in combination with current temperature responsive contrast agents only provides an ‘off-on’ signal at a certain temperature, not indicating temperature increases beyond the desired therapeutic levels. To overcome this limitation, a novel Gd-chelated hydrogel–lipid hybrid nanoparticle (HLN) formulation was developed that provides an ‘off-on-off’ signal defining a thermometric window for MR thermometry. Novel thermally responsive poly(N-isopropylacrylamide-co-acrylamide) (NIPAM-co-AM) hydrogel nanoparticles (<15 nm) with bisallylamidodiethylenetriaminetriacetic acid, a novel crosslinker with Gd³⁺ chelation functionality, were synthesized. The Gd-hydrogel nanoparticles were encapsulated in a solid lipid nanoparticle matrix that prevented T₁-weighted contrast signal enhancement. Melting of the matrix lipid freed the Gd-hydrogel nanoparticles into the bulk water and an ‘off-on’ contrast signal enhancement occurred. As the temperature was further increased to temperatures greater than, the volume phase transition temperature of the hydrogel nanoparticles, they collapsed and provided an ‘on-off’ signal diminution. Both the ‘off-on’ and the ‘on-off’ transition temperature could be tailored by changing the lipid matrix and altering the NIPAM/AM ratio in the hydrogel, respectively. This allowed MRI thermometry of different temperature windows using the Gd-HLN system.

© 2011 Elsevier B.V. All rights reserved.

1. Introduction

The potential of thermotherapy, the deposition of thermal energy, to significantly enhance the efficacy and tolerability of anti-cancer treatments has been demonstrated in several solid tumor types [1–4]. Thermotherapy can be hyperthermic or ablative depending on the applied temperature range. In hyperthermic therapy, temperatures ranging from 41 to 45 °C are produced in a target tissue for periods of minutes to hours in order to achieve cell kill, trigger drug release from drug-loaded temperature-sensitive liposomes [5–9] or induce transcription from heat sensitive transcription factors [10]. In

ablative therapy, tissue necrosis is induced through thermal coagulation at temperatures exceeding 50 °C [11].

Precise thermotherapy requires accurate thermometry of tumor and surrounding tissues during the course of heating [1, 11]. Control of spatial and temporal kinetics of heating allows the desired therapeutic effect to be achieved while sparing normal surrounding tissues [11, 12]. Needle or catheter-based thermometry has been used, but only provides a one-dimensional measure at the site of the probe tip [13]. Better temperature control throughout the three-dimensional volume of a tumor or other targeted tissue is important, because variations in the applied thermal dose significantly alter treatment outcome [12, 14], and because tumor and normal tissue are spatially and temporally heterogeneous in perfusion, and thermal and energy absorption [14]. To this end, magnetic resonance imaging (MRI) has been used to provide three-dimensional thermometry during thermotherapy [11,15,16].

MRI can provide simultaneous anatomical and local temperature information [11] through a non-invasive, non-ionizing imaging modality compatible with various heating devices [1,11,13,17,18].

* Corresponding author at: Department of Pharmaceutical Sciences, Leslie L. Dan Faculty of Pharmacy, University of Toronto, Toronto, Ontario, Canada M5S 3M2. Tel.: +1 416 978 5744; fax: +1 416 978 8511.

E-mail addresses: adam.shuhendler@utoronto.ca (A.J. Shuhendler), staruchr@sri.utoronto.ca (R. Staruch), wendy.oakden@utoronto.ca (W. Oakden), claudia.gordijo@utoronto.ca (C.R. Gordijo), rauth@uhnres.utoronto.ca (A.M. Rauth), stanisz@sri.utoronto.ca (G.J. Stanisz), chopra@sri.utoronto.ca (R. Chopra), xy.wu@phm.utoronto.ca (X.Y. Wu).

However, MR thermometry techniques that rely on the temperature dependence of water proton relaxivity or resonance frequency are highly sensitive to motion artifacts or changes in magnetic susceptibility during image acquisition [19–21]. Since these techniques derive tissue temperature from differences in pixel intensity between a baseline image and an image at elevated temperature, any local motion during or between the acquisition of the two images prevents accurate thermometry [11].

To overcome these motion artifacts, small molecule or nanoparticulate temperature-responsive contrast agents (TRCA) are used in MR thermometry [11]. Small molecule agents, including paramagnetic lanthanides [22,23], paramagnetic chemical exchange saturation transfer agents [24], and spin transition molecular materials [25,26] have been applied to MR thermometry with some success, however, all currently suffer from limitations [11,24,27]. Alternatively to small molecules are the nanoparticulate TRCA, the most investigated of which are the temperature sensitive liposomes [27–30]. In a low temperature state, the sparse access of the loaded contrast agent to free water provides minimal contrast enhancement in the MRI [28, 29]. As the local temperature is raised above the melting temperature (T_{melt}) of the lipid, the liposomal membrane becomes leaky, releasing contrast agent, increasing its exchange with bulk water and enhancing the MRI signal. The transition temperature at which this enhanced contrast occurs can be adjusted by changing the lipid composition of the liposomal membrane [27], but the non-linear relationship between contrast enhancement and temperature precludes quantitative thermometry. Moreover, these liposomal TRCA only provide an irreversible 'off-on' signal transition when the T_{melt} is reached [27], and are unable to indicate further temperature increase which may otherwise cause unwanted damage to normal tissue [27].

For effective and safe thermotherapy, detection of two temperature thresholds, *i.e.*, the lower and the upper bound, is critical. To this end, a novel thermally responsive hydrogel–lipid-hybrid nanoparticulate (HLN) system has been engineered in this work with a two-point contrast signal change. The high water solubility of the gadolinium- N,N,N',N',N'' -diethylenetriaminepentaacetic acid (Gd-DTPA) complex would result in rapid release to the aqueous bulk, precluding stable loading of the chelated contrast agent into the hydrogel nanoparticles. In order to achieve stable loading of Gd in hydrogel nanoparticles, a novel cross-linker with metal chelation functionality was synthesized, allowing for the covalent incorporation of a metal chelator into the constituent copolymer of the hydrogel nanoparticle. The novel cross-linker allowed for the synthesis of ultrasmall, thermally-responsive, stable Gd-chelating hydrogel nanoparticles. These Gd-loaded hydrogels were then loaded into larger solid lipid nanoparticles to form the HLN. Upon heating, the melting of the lipid component of the HLN and release of the Gd^{3+} -loaded hydrogels into the surrounding bulk fluid resulted in an 'off-on' contrast enhancement transition. With further heating beyond the volume phase transition temperature (T_{tr}) of the hydrogel nanoparticles, an 'on-off' diminution of contrast signal enhancement occurred. Since both the hydrogels and the solid lipid nanoparticles possess customizable T_{tr} and T_{melt} , respectively, a temperature window can be tailored to the specific thermal regimen necessary for individual patient thermotherapy.

2. Experimental

2.1. Chemicals and reagents

DTPA, allylamine, eicosanoic acid, xylol orange, gadolinium (III) chloride, acrylamide (AM), poly(ethylene glycol)-100-stearate (Myrj59), poly(ethylene glycol)-40-stearate (Myrj 52), cupric acetate, potassium persulfate, sodium dodecyl sulfate (SDS), myristic acid, ethanol (EtOH), methanol, isopropanol, acetonitrile, pyridine (Py), and acetic anhydride (AcAn) were purchased from Sigma-Aldrich Inc. (Oakville, Ontario, Canada) and used without further purification. N-isopropyl

acrylamide (NIPAM) was purchased from Monomer-Polymer & Dajac Labs Inc. (Feasterville, PA, USA). Pluronic F68 was purchased from BASF (Mississauga, Ontario, Canada). Deuterated nuclear magnetic resonance (NMR) solvents, including deuterated dimethylsulfoxide (DMSO-d_6) and deuterium oxide (D_2O) were purchased from Cambridge Isotopes Laboratories, Inc. (Andover, MA, USA).

2.2. Synthesis and characterization of N,N' -bisallylamidodiethylenetriamine- N,N',N'' -triacetic acid (BADTTA)

Using a similar method as previously described [31–33], DTPA was dehydrated to form DTPA bisanhydride by reaction with pyridine and acetic anhydride in acetonitrile at 60 °C for 12 h (Fig. 1A). After the recovery of DTPA bisanhydride and the verification of its purity with a standard $^1\text{H-NMR}$ pulse sequence using a Varian Mercury 300 MHz instrument (Agilent Technologies Canada, Inc., Mississauga, ON, Canada) (data not shown), DTPA bisanhydride was mixed with acetonitrile and isopropanol. Following the addition of allylamine in two-fold molar excess to DTPA bisanhydride, the mixture was stirred overnight at 45 °C. BADTTA was isolated and the structure was confirmed by standard proton (^1H), carbon (^{13}C), and ^1H - ^1H gradient correlations spectroscopy (GCOSy) NMR pulse sequences on a Varian Mercury 300 MHz instrument. BADTTA and DTPA were titrated in 0.1 mM potassium chloride with 0.1 M potassium hydroxide. Acid dissociation constant (pK_a) values were calculated from the generated curves using CurTiPot© Software (Gutz, I., University of São Paulo, São Palo, Brazil).

2.3. Synthesis and characterization of hydrogel nanoparticles

Hydrogel nanoparticles of poly(NIPAM-co-AM) with well-characterized thermoresponsive properties and biocompatibility were synthesized by emulsion polymerization in aqueous surfactant solution, with modification of methods previously published [34, 35]. NIPAM and AM monomer were added to each reaction to a total of 0.05 mol. SDS (0.24 g) and BADTTA (0.31 g) were added, followed by 400 mL of distilled, deionized water heated to 60 °C and bubbled with nitrogen gas. After 30 min, polymerization was initiated with potassium persulfate and allowed to continue for 60 min at 60 °C. Then the suspension of

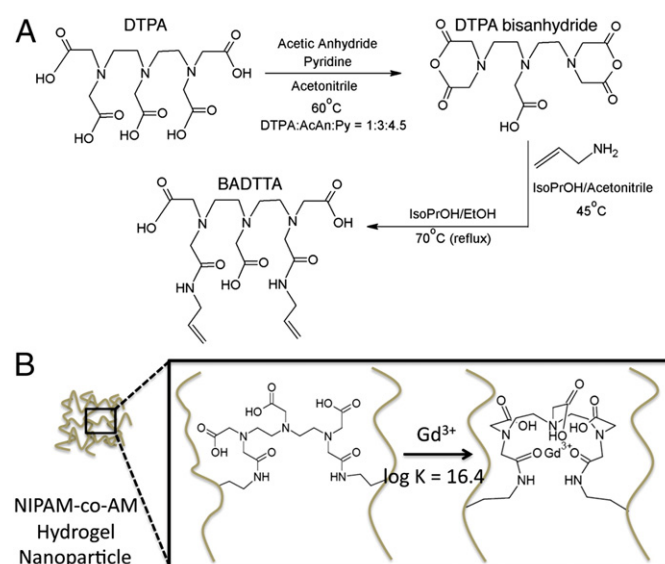


Fig. 1. Synthesis of the novel chelator-cross linker BADTTA. (A) The novel chelator-cross linker BADTTA was synthesized through the dehydration of DTPA, and subsequent reaction with allylamine. (B) A schematic diagram of the cross-linking of copolymer chains (brown) by BADTTA, and the putative structure of Gd^{3+} bound to the chelator. The dissociation constant of $\log K_D = 16.4$ is given.

hydrogel nanoparticles were cooled and dialyzed overnight. The resultant hydrogel nanoparticles contained BADTTA as crosslinker, imparting novel metal chelating capability to this formulation (Fig. 1B). The size of the hydrogel nanoparticles was measured by dynamic light scattering (Nicomp 380 Zetasizer, Particle Sizing Systems, Port Richey, FL, USA) and by transmission electron microscopy on uranyl acetate-counterstained samples using an Hitachi H7000 microscope at 75 kV (Hitachi High Technologies America Inc., Pleasanton, CA, USA). Gd was loaded into the hydrogels by incubating them with 0.5% w/w Gd for 120 min. The excess Gd was removed by repeated washings in distilled, deionized water. To ensure Gd removal, samples of washing were assayed for Gd content with xylenol orange. The dissociation constant of the hydrogel nanoparticles towards Gd and the loading of Gd onto the nanoparticles were determined through competitive chelation against xylenol orange as previously described [33]. The utility of Gd-loaded hydrogel nanoparticles as MRI contrast agents was assessed by calculating longitudinal relaxivity (r_1) by 2D inversion recovery using a 1.5 T GE MR scanner (Signa, GE Healthcare, WI, USA). To control the temperature during scanning, the hydrogel nanoparticle samples were floated in a water-jacketed beaker attached to a circulating water bath (Model 1130A, VWR International, Mississauga, ON, Canada). The T_{tr} of hydrogel nanoparticles was determined by following the change of transmittance at 600 nm, as previously described [36, 37]. Temperature values ranging from 34 °C to 86 °C were used. The temperature of the solution inside the cuvette was measured using a Fluke 51 electronic thermometer (John Fluke Mfg. Co. Inc., Everett, WA, USA) and the transmittance of the suspension at 600 nm was recorded on an Agilent 8453 Spectrophotometer (Agilent Technologies Canada Inc., Mississauga, ON, Canada). A plot of the percent transmittance at 600 nm versus temperature (°C) was generated, and curves were fitted to the data using NCSS v.7 (NCSS, Kaysville, UT, USA). The T_{tr} for each hydrogel nanoparticle formulation was calculated from the point of inflections of the fitted curves.

2.4. Formulation of hydrogel–lipid hybrid nanoparticles

In order to achieve T_{melt} of the lipid matrix of HLN that were relevant to target temperatures for non-ablative and ablative thermal therapy, three HLN formulations were created, each with a lipid matrix formed from one of myristate, methyleicosanoate or ethyleicosanoate. The fatty esters were synthesized as previously described [38], and verified by standard 1H and ^{13}C NMR pulse sequences on a Varian Mercury 300 MHz instrument (Supplementary Fig. S1).

To formulate HLN, the desired lipid, Myrj59, and Myrj52 were melted at 80 °C. Myrj59 and Myrj52 provide a poly(ethylene glycol) corona around the HLN, which is well known to enhance formulation stability and biocompatibility. Once molten, maximally Gd-loaded hydrogel nanoparticle suspension in distilled deionized water was added under gentle constant stirring at 80 °C, beyond the T_{tr} of the hydrogel nanoparticles, to maximize partitioning of these nanoparticles into the molten hydrophobic lipid–surfactant mixture (Supplementary Fig. S2). After the addition of Pluronic F68, the hot emulsion was sonicated for 5 min using a Hielscher UP-100S probe sonicator (Hielscher USA, Inc., Ringwood, NJ, USA), and quickly dispersed into cold 0.9% sodium chloride solution and stirred gently for 5 min. The particle size was measured by dynamic light scattering using a NICOMP Zetasizer 380 (Particle Sizing Systems, Inc., Morrisville, PA, USA). After freeze drying, the Gd loading capacity of HLN was analyzed by inductively coupled plasma atomic absorption spectroscopy (Optima 7300 ICP AES, PerkinElmer Inc., Waltham, MA, USA).

2.5. Temperature-sensitive magnetic resonance contrast enhancement of HLN

In order to demonstrate the MR thermometric capability of HLN, aliquots of HLN suspensions were placed into 2 mL microcentrifuge

tubes (VWR Canada, Mississauga, ON, Canada). These tubes were heated in a hot water bath at temperatures ranging from 30 °C to 65 °C for 10 min, vortex mixed, and rapidly cooled on ice. The T_1 -weighted relaxivity of the solutions were then measured on a 1.5 T MRI scanner (GE Signa, GE Medical Systems, Milwaukee, WI, USA) using a standard inversion recovery spin echo sequence. Sequence parameters were: repetition time (TR) 2500 ms, echo time (TE) 9 ms, nine inversion times (TI = 50, 350, 650, 950, 1250, 1550, 1850, 2150, and 2450 ms), $0.9 \times 0.9 \times 4$ mm voxel size. Data analysis was performed using Matlab (The MathWorks Inc, Natick, MA, USA). Regions of interest were drawn for each sample and a signal containing an average of 20 voxels was evaluated for each TI. The signal to noise ratio was approximately 200. For illustration purposes a T1-weighted spoiled gradient echo image was acquired with TR 5.3 ms, TE 1.4 ms, flip angle 30°, $0.9 \times 0.9 \times 4$ mm voxels, 40 averages.

3. Results

3.1. Synthesis and characterization of the chelator–cross linker BADTTA

To ensure retention of Gd within hydrogel nanoparticles, a novel cross-linker BADTTA with the ability to chelate Gd with high affinity was synthesized (Fig. 1A). DTPA is a clinically applied chelator of Gd with high specificity and high affinity for the lanthanide metal [39]. By synthesizing a cross-linker from DTPA, tight Gd binding capability was combined with the ability of this novel chelator to be covalently incorporated into the hydrogel polymer structure (Fig. 1B). To this end DTPA was dehydrated to form a symmetrical bisanhydride, providing two nucleophilic reactive centers per DTPA molecule. Allylamine was then conjugated to DTPA bisanhydride, providing the chelator with cross-linking functionality for free radical-mediated polymerization reactions. The structure of BADTTA was confirmed with 1H and ^{13}C NMR (Fig. 2) and with 1H - 1H GCOSy NMR (Supplementary Fig. S3).

The pK_a values of the tri-carboxylic acid molecule BADTTA were determined to be 9.55, 4.40, and 2.66 with potentiometric titration. These values are close to the pK_a values obtained for DTPA (10.11, 8.30, 4.04, 2.49, 1.92) within 5% of previously reported values [33]. The definition of only three pK_a further confirms the successful bisamidation of DTPA with allylamine [33].

3.2. Thermal properties of Gd-loaded BADTTA cross-linked N-isopropylacrylamide-co-acrylamide hydrogel nanoparticles

Three different NIPAM-co-AM hydrogel nanoparticle formulations were synthesized using BADTTA, and their thermal properties were determined. Table 1 shows that as the amount of AM increased in the NIPAM:AM mol ratio from 35% to 37.5% to 40%, the T_{tr} values of the resultant hydrogel nanoparticles increased from 54 °C, to 56 °C, and to 60 °C. The nanoparticles were uniform in size and shape, as indicated by the representative TEM micrograph of the 60:40 NIPAM:AM formulation (Supplementary Fig. S4), with hydrodynamic diameters of 10–14 nm (Table 1). The dissociation constant ($\log K_d$) of the BADTTA-containing hydrogels, a measure of the affinity of the novel chelator cross-linker for Gd, was determined to be 16.4. Although this value is less than the $\log K_d$ of DTPA (22.3), it is large enough to ensure the biocompatibility of the chelator–metal complex [33].

3.3. Relaxivities of Gd-loaded hydrogel nanoparticles

With the demonstrated affinity of the hydrogel nanoparticles for Gd, and the good loading capacity of the particles of 0.004 g of Gd per g of hydrogel nanoparticle, the *in vitro* relaxivity of the Gd-loaded hydrogels was assessed relative to solutions of DTPA and BADTTA (Table 1). The longitudinal relaxivity (r_1) is a measure of the ability of an MRI contrast agent to generate a contrast signal enhancement.

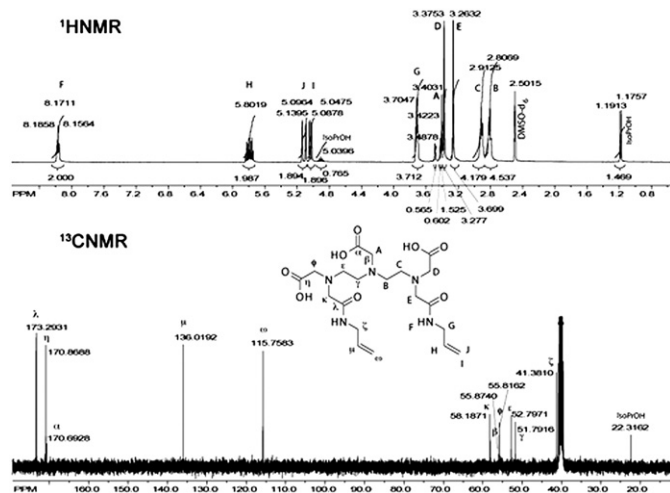


Fig. 2. Characterization of BADTTA by NMR spectroscopy. ^1H (top) and ^{13}C (bottom) NMR of BADTTA in DMSO-d_6 . The structure of BADTTA given has protons and carbons labeled by English and Greek alphabet symbols, respectively, which correspond to the represented moiety on BADTTA.

The r_1 for Gd-DTPA and Gd-BADTTA were found to be $4.0 \text{ mM}^{-1} \text{ s}^{-1}$ and $3.8 \text{ mM}^{-1} \text{ s}^{-1}$, respectively, at 20°C , in agreement with the r_1 value for Gd-DTPA previously reported [39]. For all hydrogel formulations, there was an approximate 3-fold enhancement in the r_1 values at room temperature over Gd-DTPA (Table 1). However, when the temperature of the solution was raised to the respective T_{tr} plus 7°C for each of the hydrogel formulations, there was a significant decrease of $\sim 30\%$ in the r_1 values (Table 1).

3.4. Hydrogel–lipid hybrid nanoparticles undergo ‘off-on’ and ‘on-off’ MR transitions

The thermally-responsive, Gd-loaded hydrogel nanoparticles were successfully encapsulated into the hydrophobic matrix of solid lipid nanoparticles to form HLN as illustrated in Supplementary Fig. S2. Three HLN formulations were prepared by varying the monomer composition of the loaded hydrogel, respectively containing 60:40, 62.5:37.5, and 65:35 mol NIPAM:AM. No significant difference in particle size was found between the three HLN types (Table 2). After extensive washing of the formed HLN with distilled deionized water, the Gd contents of each of the three HLN formulations were quantified, with similar loading levels (Table 2).

The ability of HLN to act as TRCA for MR thermometry was assessed *in vitro* by incubating aliquots of the HLN formulations at a given temperature under gentle mixing, followed by cooling before MRI (Figs. 3 and 4). In the first round of experiments, HLN were all loaded with hydrogel nanoparticles containing 65:35 mol NIPAM:AM, but varying the T_{melt} of the lipid matrix (Fig. 3A and B). The T_{melt} of ethyleicosanoate HLN (40 to 42°C) coincides with the onset of non-ablative thermal therapy, that of methyleicosanoate HLN (44 to 46°C) coincides with the upper limits of non-ablative thermal therapy, and that of myristate HLN (52 to 56°C) coincides with ablative thermal therapy. The increase in the MRI contrast enhancement from each of the three HLN formulations corresponded with the onset of the T_{melt} range of the lipids, as indicated by the color-matched arrows above the signal intensity versus temperature curves (Fig. 3A), and by the solid color-matched lines in the T_1 -weighted images of the HLN solutions (Fig. 3B). At $T < T_{\text{melt}}$, there was very little contrast enhancement observed for the intact HLN (Fig. 3). This indicated that the effect of Gd on the longitudinal relaxation of water protons was shielded and the hydrogel nanoparticles were isolated

from water within the hydrophobic core of the HLN. However, at $T > T_{\text{melt}}$ of the matrix lipid, there was a clear ‘off-on’ contrast signal enhancement that was significant enough to be discernable by the naked eye when examining the T_1 -weighted image (Fig. 3B). In addition, there was a decrease in the MRI signal that appeared to be associated with the T_{tr} of the HLN-encapsulated hydrogel nanoparticle, as indicated by the dotted orange arrow (Fig. 3A) and dotted orange line (Fig. 3B). The overall contrast signal enhancement of the myristate HLN is lower than the ethyleicosanoate or methyleicosanoate HLN formulations (Fig. 3).

To investigate the effect of hydrogel T_{tr} on the decrease in signal intensity of the HLN formulations, a second round of experiments was performed with the same matrix lipid (ethyleicosanoate), but varying NIPAM:AM ratio in the hydrogel, changing the associated T_{tr} , as shown in Table 1. As expected, at the T_{melt} of the HLN matrix lipid (40 to 42°C), indicated in Fig. 4A by the solid orange arrow and in Fig. 4B by the solid orange line, there was a significant enhancement of the MRI signal contrast (Fig. 4). When HLN were incubated at $T > T_{\text{tr}}$ of their loaded hydrogels, there was an ‘on-off’ decrease in MRI signal intensity discernable with the naked eye (Fig. 4B). As the T_{tr} of the 65:35 (green triangle), 62.5:37.5 (blue diamond), and 60:40 (red squares) mol NPAM:AM hydrogels increased from 54°C to 56°C to 60°C , respectively, the ‘on-off’ temperature increased (Fig. 4). This result indicated that both the lipid matrix T_{melt} of the HLN, as well as the T_{tr} of the loaded hydrogel nanoparticles, contribute to ‘off-on’ and ‘on-off’ MRI contrast signal change, respectively.

4. Discussion

A novel hybrid nanoparticle formulation, the HLN, comprised of thermally responsive, Gd chelator-crosslinked hydrogel nanoparticles loaded into solid lipid nanoparticles has been formulated with the demonstrated ability to define a customizable temperature window for MR thermometry. The novel polymerizable metal chelator was synthesized to meet the two main requirements of Gd-based MRI contrast agents: (i) Gd must be tightly bound to the chelator as free Gd in the body is toxic; and (ii) the Gd complex must have a coordinated water molecule in fast exchange with the bulk water [40]. DTPA is a clinically used Gd chelator, however, the high water solubility of Gd-DTPA complexes are not amenable to stable loading inside a hydrogel nanoparticle. However, the novel chelator-cross linker BADTTA can be covalently incorporated into the hydrogel copolymer to provide stable Gd chelation, allowing for retention of chelated Gd within the hydrogel nanoparticles.

The synthesis of BADTTA through the bisamidation of DTPA results in products that possess both tight Gd binding and water coordination characteristics [31, 33, 41, 42], with the amide carbonyl oxygens, reducing calcium chelation affinity of the bisamide approximately 3 log units relative to native DTPA [42]. In preserving the MRI contrast agent characteristics of DTPA, the alkene groups BADTTA impart the

Table 1
Characterization of novel Gd-chelating, temperature responsive hydrogel nanoparticles.

	Hydrated formulation (mol NIPAM: mol AM)		
	60:40	62.5:37.5	65:35
Hydrodynamic diameter (nm)	12 (0.28)	10 (0.24)	14 (0.17)
Loading capacity (g Gd/g hydrogel)	0.004 (0.001)	0.004 (0.001)	0.004 (0.001)
Relaxivity at 20°C ($\text{s}^{-1} \text{mM}^{-1}$)	12.4	12.6	12.2
Relaxivity at $T_{\text{tr}} + 7^\circ\text{C}$ ($\text{s}^{-1} \text{mM}^{-1}$)	8.6	7.8	7.6
T_{tr} $^\circ\text{C}$	54	56	60

Hydrodynamic diameters and loading capacities are given as the mean (polydispersity index) of three measurements. The relaxivity of Gd-DTPA was $4.0 \text{ mM}^{-1} \text{ s}^{-1}$ and for Gd-BADTTA was $3.8 \text{ mM}^{-1} \text{ s}^{-1}$ at 20°C .

Table 2
Characterization of Gd-hydrogel-loaded HLN.

	Encapsulated hydrogel (mol NIPAM: mol AM)		
	60:40	62.5:37.5	65:35
Hydrodynamic diameter (nm)	109 (0.82)	112 (0.66)	104 (0.73)
Loading capacity (% Gd w/w)	0.49	0.45	0.48

Hydrodynamic diameters are given as the mean (polydispersity index) of three measurements.

extra functionality of covalently incorporating the chelator into polymer hydrogels (Fig. 1B).

The decreased dissociation constant of BADTTA (16.4) relative to DTPA (22.6) [33] was expected due to the change of the pK_a values between these chelators following bisamidation, as previously demonstrated for other DTPA bisamides [33]. The dissociation constant of BADTTA for Gd is still sufficiently strong, though, to afford *in vivo* application, especially in light of the enhanced Gd binding specificity afforded by the bisamidation.

In addition to Gd chelation, BADTTA-cross linked poly(NIPAM-co-AM) hydrogels also possessed tunable thermal sensitivity, which reduced the MRI contrast of the hydrogels beyond a given T_{tr} and resulted in their TRCA properties. The thermal sensitivity of poly(NIPAM-co-AM) hydrogels is well known and characterized [43], which is the result of a balance of swelling-favorable mixing entropy and deswelling-favorable mixing interactions [44, 45]. At T > T_{tr}, deswelling predominates and NIPAM-co-AM polymer chains lose as much as 80% of bound water content [43, 46]. Since Gd is chelated throughout the hydrogel and since the MRI contrast enhancement of Gd-based contrast agents requires the rapid exchange of coordination sphere water with bulk water [47], this T_{tr}-associated polymer chain dehydration would reasonably decrease access of Gd to free water, thus lowering the contrast signal enhancement. For all three hydrogel nanoparticle formulations, the r₁ of the formulation

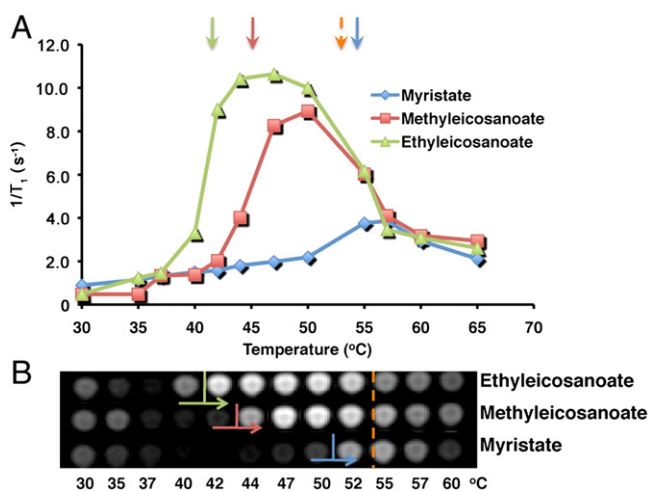


Fig. 3. HLN provides ‘off-on’ signal for MRI thermometry *in vitro*. The water proton relaxation rate ($1/T_1$) as a function of temperature was determined, *in vitro*, for HLN formulations with different matrix lipids [myristate (blue diamond), methylcoisanoate (red squares), and ethyleicoisanoate (green triangles)], each with different melting temperatures indicated by solid arrows above the curve. The arrows are color-matched to the curves they relate to, and the orange arrows indicate the T_{tr} of the common hydrogel composition (65:35 mol NIAPM:AM) used. The T₁-weighted contrast enhancement provided by each HLN formulation as a function of temperature are shown (B). The solid indicate lipid melting temperatures of ethyleicoisanoate (green), methylcoisanoate (red), and myristate (blue), the arrows indicate a signal enhancement transition, and the dashed orange line indicates hydrogel T_{tr}.

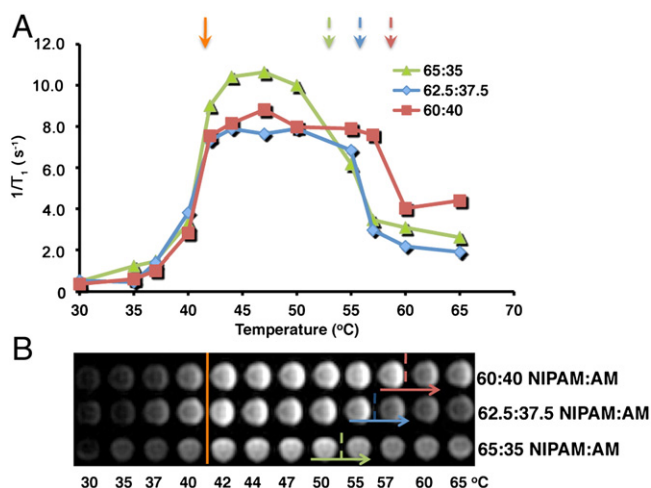


Fig. 4. HLN also provide ‘on-off’ signal for MRI thermometry *in vitro*. The water proton relaxation rate ($1/T_1$) as a function of temperature was determined, *in vitro*, for HLN formulations with varying NIPAM:AM composition hydrogel nanoparticles, from 65:35 (green triangles), to 62.5:37.5 (blue diamonds), to 60:40 (red squares). The T_{tr} of the hydrogel nanoparticles are indicated by dashed arrows above the curves. The arrows are color-matched to the curves they relate to, and the orange arrows indicate the melting temperature of the common matrix lipid (ethyleicoisanoate) used in all three formulations. The T₁-weighted contrast signal decrease provided by each HLN formulation as a function of temperature is shown (B). The dashed lines indicate the T_{tr} of the hydrogel nanoparticle, with 65:35 (green), 62.5:37.5 (blue), and 60:40 mol NIPAM:AM (red), the arrows indicate a signal enhancement transition, and the solid orange line indicates the lipid melting temperature.

decreased approximately 30% upon heating above the respective hydrogel-associated T_{tr} (Table 1).

The Gd-loaded NIPAM-co-AM hydrogel nanoparticles also possessed a stronger contrast enhancement (approx. 12 mM⁻¹ s⁻¹) relative to both DTPA-Gd (4.0 mM⁻¹ s⁻¹) and BADTTA-Gd (3.8 mM⁻¹ s⁻¹) complexes (Table 1). This contrast enhancement is well known for macromolecular contrast agents [39]. This contrast enhancement of macromolecular Gd chelates is inversely proportional to the rate of rotation of the chelated metal [47]. Since random molecular motion is dependent on the size of the molecule, macromolecules inherently slow the rotational motion of the Gd complex, enhancing the relaxivity of the contrast agent, as was observed for the hydrogel nanoparticles synthesized here.

A schematic representing the proposed mechanism of thermometry by HLN is shown in Fig. 5. At T < T_{tr} and T < T_{melt}, (Fig. 5 panel 1), the hydrogel-chelated Gd is unable to interact with bulk water and unable to produce T₁-weighted contrast signal enhancement. At T > T_{melt} but T < T_{tr}, (Fig. 5 panel 2), the hydrogel preferentially partitions into the bulk water, allowing the free diffusion of water throughout the hydrogel to maximize interactions with chelated Gd, resulting in an ‘off-on’ contrast signal enhancement (Figs. 3 and 4). The onset of this ‘off-on’ transition was also demonstrated to be tunable by changing the lipid forming the HLN matrix (Fig. 3). Therefore, depending on whether non-ablative (~43 °C) or ablative (>50 °C) heating regimes are required, the ‘off-on’ signal can be customized by changing the matrix lipid.

With temperature sensitive liposomes, heating beyond the initial ‘off-on’ transition does not result in any further meaningful thermometric information [27]. However, continued heating of HLN to T > T_{tr} results in an ‘on-off’ T₁-weighted contrast signal decrease (Fig. 4), which may be the result (i) the 30% decrease in r₁ due to the volume phase transition at the T_{tr} (Table 1); and (ii) the limited interaction of chelated Gd with bulk water molecules due to partitioning of the hydrogel into lipophilic environments, such as fatty tissue or molten lipid droplets (Fig. 5 panel 3). This ‘on-off’ transition,

by any mechanism, is dependent on the T_{tr} of the hydrogel nanoparticle (Fig. 4). Since the T_{tr} can be modified by altering the NIPAM:AM ratio of the hydrogel copolymers (Table 1), the 'on-off' contrast signal transition can be customized to a given temperature threshold. A proof of this principle has been demonstrated, illustrating the potential of the HLN as a TRCA capable of two temperature point, absolute temperature thermometry in the MRI (Figs. 3 and 4).

While the two-point thermometry of HLN has only been demonstrated *in vitro*, evidence exists to support the successful implementation of this system *in vivo* for rapid, three-dimensional T_1 -weighted MR thermometry. The novel Gd-chelating hydrogel nanoparticle is afforded an enhanced relaxivity ($r_1 = 12.4 \text{ mM}^{-1} \text{ s}^{-1}$) relative to clinically applied small molecule contrast agents, reducing the concentration required for contrast agent detection in the MRI. For dendrimer-based Gd chelators with $r_1 = 10.7 \text{ mM}^{-1} \text{ s}^{-1}$, the lower limit of detection for rapid T_1 -weighted MRI was reported to be $9 \pm 3 \mu\text{M}$ of chelated Gd [48]. As the relaxivity of the hydrogel nanoparticles is greater than the dendrimer contrast agent, this lower concentration limit is expected to become even lower and the HLN should provide detectable MRI contrast signals for rapid, three-dimensional T_1 -weighted imaging. In addition to the enhanced relaxivity, the nanoparticulate nature of the HLN can promote tumor accumulation and retention of the contrast agent through the enhanced permeability and retention effect [49, 50], enhancing tumor-specific concentrations of this TRCA. Through this effect, it is possible that the tumor accumulation of the HLN will exceed the proposed low micromolar lower detection limit for adequate signal evolution in the MRI. In this light, continuing investigations will assess the utility of HLN for *in vivo* MRI thermometry.

5. Conclusions

The synthesis of BADTTA, a novel chelator with cross-linking functionality, and its incorporation into NIPAM-co-AM hydrogel nanoparticles loaded into solid lipid nanoparticles (HLN) provides two-temperature-point thermometry in the MRI. The 'off-on' T_1 -weighted contrast signal enhancement provided by the solid lipid nanoparticle was customizable by changing the lipid composition of the matrix. Similarly, the 'on-off' contrast signal decrease attributable to the T_{tr} of the hydrogel nanoparticles could also be adjusted by modifying the NIPAM:AM ratio of the hydrogel. This nanoparticle-in-a-nanoparticle system could allow for absolute thermal window definition with the ability to customize both the low and high temperature threshold values.

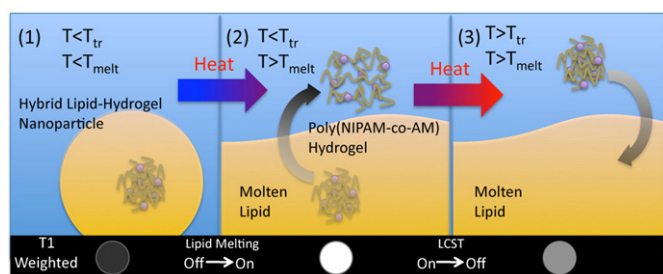


Fig. 5. The proposed mechanism for the two-point thermometry provided by HLN. (1) At temperatures (T) below the lower volume phase transition temperature (T_{tr}) of the hydrogel nanoparticles and below the melting temperature (T_{melt}) of matrix lipid, the Gd-loaded hydrogel nanoparticles remained trapped within the solid hydrophobic core of the HLN, and are unable to interact with bulk water molecules. (2) At $T > T_{melt}$ of the matrix lipid, but below the hydrogel T_{tr} , the hydrophilic hydrogel nanoparticle can interact with the bulk water to produce a T_1 -weighted signal enhancement, providing 'off-on' triggers to define the lower end of the temperature window. (3) At $T > T_{tr}$, the hydrogel becomes hydrophobic, limiting the interaction of Gd with the bulk water and reducing the T_1 -weighted contrast signal enhancement, providing the 'on-off' signal decrease that defines the upper end of the temperature window.

Acknowledgments

This work was partly supported by a Discovery Grant from the National Science and Engineering Research Council of Canada to X.Y. Wu. Scholarships to AJS are provided by the National Science and Engineering Research Council of Canada, and the University of Toronto Ben Cohen Fund are also acknowledged.

Appendix A. Supplementary data

Supplementary data to this article can be found online at doi:10.1016/j.jconrel.2011.09.061.

References

- [1] B.D. de Senneville, C. Mougenot, B. Quesson, I. Dragonu, N. Grenier, C.T. Moonen, MR thermometry for monitoring tumor ablation, *Eur. Radiol.* 17 (2007) 2401–2410.
- [2] J.A. Marrero, Hepatocellular carcinoma, *Curr. Opin. Gastroenterol.* 22 (2006) 248–253.
- [3] H. Furusawa, K. Namba, S. Thomsen, F. Akiyama, A. Bendet, C. Tanaka, Y. Yasuda, H. Nakahara, Magnetic resonance-guided focused ultrasound surgery of breast cancer: reliability and effectiveness, *J. Am. Coll. Surg.* 203 (2006) 54–63.
- [4] T. Uchida, H. Ohkusa, H. Yamashita, S. Shoji, Y. Nagata, T. Hyodo, T. Satoh, Five years experience of transrectal high-intensity focused ultrasound using the Sonablate device in the treatment of localized prostate cancer, *Int. J. Urol.* 13 (2006) 228–233.
- [5] M. de Smet, E. Heijman, S. Langereis, N.M. Hijnen, H. Grull, Magnetic resonance imaging of high intensity focused ultrasound mediated drug delivery from temperature-sensitive liposomes: an *in vivo* proof-of-concept study, *J. Control. Release* 150 (2011) 102–110.
- [6] M. de Smet, S. Langereis, S. van den Bosch, H. Grull, Temperature-sensitive liposomes for doxorubicin delivery under MRI guidance, *J. Control. Release* 143 (2010) 120–127.
- [7] R. Staruch, R. Chopra, K. Hynynen, Localised drug release using MRI-controlled focused ultrasound hyperthermia, *Int. J. Hyperthermia* 27 (2011) 156–171.
- [8] T. Tagami, M.J. Ernsting, S.D. Li, Efficient tumor regression by a single and low dose treatment with a novel and enhanced formulation of thermosensitive liposomal doxorubicin, *J. Control. Release* 152 (2011) 303–309.
- [9] A. Yudina, M. de Smet, M. Lepetit-Coiffe, S. Langereis, L. Van Ruijssevelt, P. Smirnov, V. Bouchaud, P. Voisin, H. Grull, C.T. Moonen, Ultrasound-mediated intracellular drug delivery using microbubbles and temperature-sensitive liposomes, *J. Control. Release* (Jun 12 2011) [Epub ahead of print].
- [10] D.P. Madio, P. van Gelderen, D. DesPres, A.W. Olson, J.A. de Zwart, T.W. Fawcett, N.J. Holbrook, M. Mandel, C.T. Moonen, On the feasibility of MRI-guided focused ultrasound for local induction of gene expression, *J. Magn. Reson. Imaging* 8 (1998) 101–104.
- [11] V. Rieke, K. Butts Pauly, MR thermometry, *J. Magn. Reson. Imaging* 27 (2008) 376–390.
- [12] S.A. Sapareto, W.C. Dewey, Thermal dose determination in cancer therapy, *Int. J. Radiat. Oncol. Biol. Phys.* 10 (1984) 787–800.
- [13] C.T.W. Moonen, MR temperature mapping in local drug delivery and thermotherapy, *Med. Mundi* 44 (2000) 34–42.
- [14] C.A. Perez, S.A. Sapareto, Thermal dose expression in clinical hyperthermia and correlation with tumor response/control, *Cancer Res.* 44 (1984) 4818s–4825s.
- [15] Y. Ishihara, A. Calderon, H. Watanabe, K. Okamoto, Y. Suzuki, K. Kuroda, Y. Suzuki, A precise and fast temperature mapping using water proton chemical shift, *Magn. Reson. Med.* 34 (1995) 814–823.
- [16] N.J. McDannold, R.L. King, F.A. Jolesz, K.H. Hynynen, Usefulness of MR imaging-derived thermometry and dosimetry in determining the threshold for tissue damage induced by thermal surgery in rabbits, *Radiology* 216 (2000) 517–523.
- [17] R. Chopra, N. Baker, V. Choy, A. Boyes, K. Tang, D. Bradwell, M.J. Bronskill, MRI-compatible transurethral ultrasound system for the treatment of localized prostate cancer using rotational control, *Med. Phys.* 35 (2008) 1346–1357.
- [18] R. Chopra, L. Curie, R. Staruch, L. Morrison, K. Hynynen, An MRI-compatible system for focused ultrasound experiments in small animal models, *Med. Phys.* 36 (2009) 1867–1874.
- [19] J. De Poorter, Noninvasive MRI thermometry with the proton resonance frequency method: study of susceptibility effects, *Magn. Reson. Med.* 34 (1995) 359–367.
- [20] R.D. Peters, R.M. Henkelman, Proton-resonance frequency shift MR thermometry is affected by changes in the electrical conductivity of tissue, *Magn. Reson. Med.* 43 (2000) 62–71.
- [21] S.M. Sprinkhuizen, M.K. Konings, M.J. van der Bom, M.A. Viergeever, C.J. Bakker, L.W. Bartels, Temperature-induced tissue susceptibility changes lead to significant temperature errors in PRFS-based MR thermometry during thermal interventions, *Magn. Reson. Med.* 64 (2010) 1360–1372.
- [22] S.K. Hekmatyar, R.M. Kerkhoff, S.K. Pakin, P. Hopewell, N. Bansal, Noninvasive thermometry using hyperfine-shifted MR signals from paramagnetic lanthanide complexes, *Int. J. Hyperthermia* 21 (2005) 561–574.
- [23] S.K. Pakin, S.K. Hekmatyar, P. Hopewell, A. Babsky, N. Bansal, Non-invasive temperature imaging with thulium 1,4,7,10-tetraazacyclododecane-1,4,7,10-tetramethyl-1,4,7,10-tetraacetic acid (TmDOTMA-), *NMR Biomed.* 19 (2006) 116–124.

- [24] D.E. Woessner, S. Zhang, M.E. Merritt, A.D. Sherry, Numerical solution of the Bloch equations provides insights into the optimum design of PARACEST agents for MRI, *Magn. Reson. Med.* 53 (2005) 790–799.
- [25] R.N. Muller, L. Vander Elst, S. Laurent, Spin transition molecular materials: intelligent contrast agents for magnetic resonance imaging, *J. Am. Chem. Soc.* 125 (2003) 8405–8407.
- [26] F. Settecase, M.S. Sussman, T.P. Roberts, A new temperature-sensitive contrast mechanism for MRI: Curie temperature transition-based imaging, *Contrast Media Mol. Imaging* 2 (2007) 50–54.
- [27] L.H. Lindner, H.M. Reinl, M. Schlemmer, R. Stahl, M. Peller, Paramagnetic thermosensitive liposomes for MR-thermometry, *Int. J. Hyperthermia* 21 (2005) 575–588.
- [28] M. Peller, A. Schwerdt, M. Hossann, H.M. Reinl, T. Wang, S. Sourbron, M. Ogris, L.H. Lindner, MR characterization of mild hyperthermia-induced gadodiamide release from thermosensitive liposomes in solid tumors, *Invest. Radiol.* 43 (2008) 877–892.
- [29] J.A. Tashjian, M.W. Dewhirst, D. Needham, B.L. Viglianti, Rationale for and measurement of liposomal drug delivery with hyperthermia using non-invasive imaging techniques, *Int. J. Hyperthermia* 24 (2008) 79–90.
- [30] S.L. Fossheim, K.A. Il'yasov, J. Hennig, A. Bjornerud, Thermosensitive paramagnetic liposomes for temperature control during MR imaging-guided hyperthermia: in vitro feasibility studies, *Acad. Radiol.* 7 (2000) 1107–1115.
- [31] L. De Learie, W.H. Lin, D.A. Moore, D.H. White, Process for Manufacturing DTPA-bis Amide Magnetic Resonance Imaging, Mallickrodt Medical, Mallickrodt Medical, Inc., United States, 1996.
- [32] C.H. Paik, M.A. Ebbert, P.R. Murphy, C.R. Lassman, R.C. Reba, W.C. Eckelman, K.Y. Pak, J. Powe, Z. Steplewski, H. Koprowski, Factors influencing DTPA conjugation with antibodies by cyclic DTPA anhydride, *J. Nucl. Med.* 24 (1983) 1158–1163.
- [33] A.D. Sherry, W.P. Cacheris, K.T. Kuan, Stability constants for Gd³⁺ binding to model DTPA-conjugates and DTPA-proteins: implications for their use as magnetic resonance contrast agents, *Magn. Reson. Med.* 8 (1988) 180–190.
- [34] J. Moselhy, X.Y. Wu, R. Nicholov, K. Kodaria, In vitro studies of the interaction of poly(NIPAm/MAA) nanoparticles with proteins and cells, *J. Biomater. Sci. Polym. Ed.* 11 (2000) 123–147.
- [35] K. Zhang, X.Y. Wu, Modulated insulin permeation across a glucose-sensitive polymeric composite membrane, *J. Control. Release* 80 (2002) 169–178.
- [36] J.E. Chung, M. Yokoyama, T. Okano, Inner core segment design for drug delivery control of thermo-responsive polymeric micelles, *J. Control. Release* 65 (2000) 93–103.
- [37] X.Y. Wu, P.I. Lee, Preparation and characterization of thermal- and pH-sensitive nanospheres, *Pharm. Res.* 10 (1993) 1544–1547.
- [38] A.J. Shuhendler, P. Prasad, H.K. Chan, C.R. Gordijo, B. Soroushian, M. Kolios, K. Yu, P.J. O'Brien, A.M. Rauth, X.Y. Wu, Hybrid quantum dot-fatty ester stealth nanoparticles: toward clinically relevant in vivo optical imaging of deep tissue, *ACS Nano* 5 (2011) 1958–1966.
- [39] P. Caravan, J.J. Ellison, T.J. McMurry, R.B. Lauffer, Gadolinium(III) chelates as MRI contrast agents: structure, dynamics, and applications, *Chem. Rev.* 99 (1999) 2293–2352.
- [40] S. Aime, M. Chiaussa, G. Digilio, E. Gianolio, E. Terreno, Contrast agents for magnetic resonance angiographic applications: 1H and 17O NMR relaxometric investigations on two gadolinium(III) DTPA-like chelates endowed with high binding affinity to human serum albumin, *J. Biol. Inorg. Chem.* 4 (1999) 766–774.
- [41] M.S. Konings, W.C. Dow, D.B. Love, K.N. Raymond, S.C. Quay, S.M. Rocklage, Gadolinium complexation by a new DTPA-amide ligand. Amide oxygen coordination, *Inorg. Chem.* 29 (1996) 1488–1491.
- [42] C. Paul-Roth, K.N. Raymond, Amide functional group contributions to the stability of gadolinium (III) complexes: DTPA derivatives, *Inorg. Chem.* 34 (1995) 1409–1412.
- [43] H. Kogure, S. Nanami, Y. Masuda, Y. Toyama, K. Kubota, Hydration and dehydration behavior of N-isopropylacrylamide gel particles, *Colloid Polym. Sci.* 283 (2005) 1163–1171.
- [44] H.G. Schild, Poly(N-isopropylacrylamide): experiment, theory, and application, *Prog. Polym. Sci.* 17 (1992) 163–249.
- [45] M. Shibayama, T. Tanaka, Volume phase transition and related phenomena of polymer gels, *Adv. Polym. Sci.* 109 (1993) 1–62.
- [46] A.K. Lele, M.M. Hirve, M.V. Badiger, R.A. Mashelkar, Predictions of bound water content in poly(N-isopropylacrylamide) gels, *Macromolecules* 30 (1997) 157–159.
- [47] P. Caravan, N.J. Cloutier, M.T. Greenfield, S.A. McDermid, S.U. Dunham, J.W. Bulte, J.C.J. Amedio, R.J. Looby, R.M. Supkowski, W.D.J. Horrocks, T.J. McMurry, R.B. Lauffer, The interaction of MS-325 with human serum albumin and its effect on proton relaxation rates, *J. Am. Chem. Soc.* 124 (2002) 3152–3162.
- [48] K. Hanaoka, A.J. Lubag, A. Castillo-Muzquiz, T. Kodadek, A.D. Sherry, The detection limit of a Gd³⁺-based T1 agent is substantially reduced when targeted to a protein microdomain, *Magn. Reson. Imaging* 26 (2008) 608–617.
- [49] H. Maeda, The enhanced permeability and retention (EPR) effect in tumor vasculature: the key role of tumor-selective macromolecular drug targeting, *Adv. Enzyme Regul.* 41 (2001) 189–207.
- [50] H. Maeda, J. Wu, T. Sawa, Y. Matsumura, K. Hori, Tumor vascular permeability and the EPR effect in macromolecular therapeutics: a review, *J. Control. Release* 65 (2000) 271–284.